ISSN 0915-633X

NATIONAL INSTITUTE FOR FUSION SCIENCE

Electromagnetic Effects on Rippling Instability and Tokamak Edge Fluctuations

S. Murakami and H. Saleem

(Received - July 2, 1998)

NIFS-554 July 1998

RESEARCH REPORT
NIFS Series

NAGOYA, JAPAN

Electromagnetic Effects on Rippling Instability and Tokamak Edge Fluctuations

Sadayoshi MURAKAMI and Hamid SALEEM*

National Institute for Fusion Science
322-6 Oroshi-cho, Toki 509-5292, Japan

Electromagnetic effects on rippling mode are investigated as a cause of low frequency electromagnetic fluctuations in tokamak edge region. It is shown that, in a current-carrying resistive plasma, the purely growing electrostatic rippling mode can turn out to be an electromagnetic oscillatory instability. The resistivity fluctuation and temperature gradient are the main sources of this instability, which requires both parallel and perpendicular wave vectors. The Alfven waves in a coupled dispersion relation are found heavily damped in such dissipative plasmas.

KEYWORDS: resistivity fluctuations, current carrying plasma, rippling instability

§1. Introduction

Dissipative mechanisms usually cause damping of the perturbations. However in the presence of free energy sources like inhomogeneities and currents, perturbations may become unstable even in a collisional plasma. More than three decades ago, electrostatic rippling instability was studied first time in a current-carrying resistive plasma with temperature gradient.[1] The purely growing rippling mode requires both the parallel and perpendicular wave vectors. Therefore, in a high temperature fusion plasma (> keV), it is considered that such perturbations are not important because the parallel electron thermal conduction tends to equalize the temperature and so the mode is stabilized.

However, in the edge regions with low temperature, the stabilization by thermal conduction is not so large. The experimental observations of fluctuations and energy transport near the tokamak edge regions invoked the nonlinear study of rippling mode.[2] Then it was shown that the diamagnetic drift can couple with the rippling mode giving rise to oscillatory instabilities in the resistive current carrying non-uniform plasmas.[3] Parallel thermal conduction and parallel electron fluid compressibility effects were not included in this investigation.

In later studies, the rippling mode and it's relationship with dissipative drift waves were shown in a sheared magnetic field using Braginskii's equations.[4] These investigations about rippling mode have been limited to the electrostatic case only. However many experimental observations have shown the existence of low frequency electromagnetic fluctuations in the plasma edge regions.[4–9] These experimental observations invoke considerable interest in an electromagnetic analysis of the rippling mode.

In the present paper we study the electromagnetic instability in a current-carrying resistive plasma as a cause of electromagnetic fluctuation in tokamak edge plasma. The temperature gradient which is associated with the resistive fluctuations is the main source of instability in the presence of background current.

In section 2 the basic equations governing the phenomenon are derived. In section 3 the linear dispersion relation in the electrostatic limit is first considered. Then the electromagnetic dispersion relation for rippling mode is investigated where we obtain three coupled modes. In section 4 we study the parameter dependency of the electromagnetic rippling mode with changing the wave and plasma parameters. Finally in section 5, a summary of the present investigation is presented.

§2. Basic equations

We assume the external magnetic field, B_0, to be along z-axis with the stationary parallel current only by electrons, $J_{0z}(= -en_0v_{e0z})$. The pressure gradient is considered to be in the x-direction (for electron temperature $T_e = T_e(x)$ and density $n_e = n_e(x)$).

The perpendicular component of the electron fluid velocity, $\boldsymbol{V}_{e\perp}$, is

$$\boldsymbol{V}_{e\perp} \simeq \boldsymbol{V}_E + \boldsymbol{V}_D + \boldsymbol{V}_\pi, \tag{2.1}$$

where

$$\boldsymbol{V}_E = \frac{c}{B_0}\hat{\boldsymbol{z}} \times \nabla\phi,$$

$$\boldsymbol{V}_D = -\frac{c}{eB_0n_e}\hat{\boldsymbol{z}} \times \nabla(n_eT_e),$$

$$\boldsymbol{V}_\pi = -\frac{c}{eB_0n_e}\hat{\boldsymbol{z}} \times (\nabla \cdot \Pi),$$

are the $\boldsymbol{E} \times \boldsymbol{B}_0$, the diamagnetic, and the collisionless stress tensor drifts, respectively. Furthermore ϕ, c, e, and Π are the electrostatic potential, the speed of light, the elementary charge, and the collisionless stress tensor, respectively. The ideal gas law for the electron fluid has been assumed.

The parallel resistivity fluctuation, η_{1z}, is related with electron temperature by the relation

$$\eta_{1z} = -\frac{3}{2}\eta_{e0}\frac{T_{e1}}{T_{e0}}, \tag{2.2}$$

where $\eta_{e0} = \frac{1}{2}\frac{m_e\nu_{e0}}{n_{e0}e^2}$, ν_{e0} is the electron-ion collision fre-

* Permanent address: PINSTECH (NPD), P. O. Nilore, Islamabad, Pakistan.

quency and m_e is electron mass. The subscripts one and naught denote the linear and equilibrium quantities, respectively.

Then the parallel component of electron velocity perturbation is given by

$$\left(\frac{\partial}{\partial t}+\frac{\nu_{e0}}{2}\right)v_{ez1}=v_{te}^2\frac{\partial}{\partial z}[\tilde{\Phi}_1-\tilde{N}_1-1.71\tilde{T}_1]$$
$$-\frac{1}{2}\nu_{e0}v_{e0z}\left(\tilde{N}_1-\frac{3}{2}\tilde{T}_1\right)$$
$$+\frac{v_{te}^2}{c}\left(\frac{\partial}{\partial t}+\boldsymbol{V}_{D0}\cdot\nabla\right)\tilde{A}_1, \quad (2.3)$$

where $v_{te}^2=\frac{T_e}{m_e}$, $\tilde{\Phi}_1=\frac{e\phi_1}{T_{e0}}$, $\tilde{N}_1=\frac{n_{e1}}{n_{e0}}$, $\tilde{T}_1=\frac{T_{e1}}{T_{e0}}$ and $\tilde{A}_1=\frac{eA_{z1}}{T_{e0}}$ denotes the parallel vector potential perturbation. The unperturbed electron diamagnetic drift is denoted by $\boldsymbol{V}_{D0}=-(c/eB_0n_0)\hat{z}\times\nabla(n_0T_{e0})$. Equation (2.3) reduces to eq. (2) of ref. (11) in the absence of external parallel current. For purely electrostatic case in the limit $|\omega|<<\nu_{e0}$, this equation reduces to eq. (10 b) of ref. (4).

We, here, assume that the wavelength of the perturbation is much shorter than the density and temperature scale lengths and the physical variables have a variation proportional to $\exp(i\boldsymbol{k}\cdot\boldsymbol{x}-i\omega t)$, where ω and $\boldsymbol{k}$ are the frequency and wave vector, respectively. Then eq. (2.3) can be expressed as

$$\left(-i\omega+\frac{\nu_{e0}}{2}\right)v_{ez1}=iv_{te}^2k_z[\tilde{\Phi}_1-\tilde{N}_1-1.71\tilde{T}_1]$$
$$-\frac{1}{2}\nu_{e0}v_{e0z}\left(\tilde{N}_1-\frac{3}{2}\tilde{T}_1\right)$$
$$+\frac{v_{te}^2}{c}\left(-i\omega+i\boldsymbol{V}_{D0}\cdot\boldsymbol{k}\right)\tilde{A}_1. \quad (2.4)$$

The charge neutrality condition couples the perpendicular ion polarization current and the electron parallel current as

$$\omega\rho_s^2\nabla^2\tilde{\Phi}_1=-k_z\frac{J_{1z}}{en_0}, \quad (2.5)$$

where $\rho_s(=\frac{c\sqrt{m_iT_e}}{eB_0})$ is the ion Larmor radius at electron temperature and $J_{1z}(=-en_0v_{1ez})$ is the parallel current fluctuation. The Ampere's law together with eq. (2.5) gives a relation between $\tilde{A}_1$ and $\tilde{\Phi}_1$, viz

$$\tilde{A}_1=\frac{\omega ck_z}{\omega_A^2}\tilde{\Phi}_1, \quad (2.6)$$

where $\omega_A=v_Ak_z$ and $v_A(=\frac{B}{\sqrt{4\pi n_0m_i}})$ is the Alfven velocity.

The electron continuity equation gives

$$\frac{\partial n_{e1}}{\partial t}+(c/B_0)\hat{z}\times\nabla\phi_1\cdot\nabla n_{e0}+n_{e0}\frac{\partial}{\partial z}v_{e1z}=0. \quad (2.7)$$

Assuming $|\partial/\partial t|<<c|\nabla|,\omega_{pe}$, the parallel component of Ampère's law yields

$$v_{e1z}\sim(c/4\pi n_{e0}e)\nabla_\perp^2A_{z1}, \quad (2.8)$$

and the electron continuity equation for flat density profile ($\nabla n_{e0}=0$) becomes

$$\tilde{N}_1=-\frac{k_zc}{\omega}\lambda_{De}^2k_y^2\tilde{A}_1, \quad (2.9)$$

where $\lambda_{De}(=\sqrt{\frac{T_{e0}}{4\pi n_0e^2}})$ is electron Debye length.

Using energy equation of Braginskii,[10] we obtain the electron temperature perturbation as

$$\left(\omega-\omega_{0z}+i\omega_\chi\right)\tilde{T}_1=\left(\omega_T^*-0.47\rho_s^2k_y^2\omega\right)\tilde{\Phi}_1, \quad (2.10)$$

where $\omega_{0z}=v_{e0z}k_z$, $\omega_\chi=3.16\frac{v_{te}^2k_z^2}{\nu_{e0}}$, $\omega_T^*=\frac{cT_{e0}}{eB_0}k_y\kappa_T$ and κ_T is the inverse of temperature gradient scale length. Here $\omega>>\frac{m_e}{m_i}\nu_{e0}$ has been assumed and the perpendicular thermal conduction has been ignored. Furthermore, in eqs. (2.3) and (2.9), we have used the relations

$$(\boldsymbol{V}_D\cdot\nabla)v_{ez}=-\frac{1}{m_eN_e}(\nabla\cdot\Pi)_z, \quad (2.11)$$

and

$$\frac{3}{2}\boldsymbol{V}_D\cdot\nabla T_e-\frac{T_e}{n_e}\boldsymbol{V}_D\cdot\nabla n_e=-\frac{1}{n_e}\nabla\cdot\boldsymbol{q}_e, \quad (2.12)$$

where $\boldsymbol{q}_e=-\left(\frac{5n_eT_e}{2m_e\omega_e}\right)z\times\nabla T_e$ is the Righi-Leduc electron heat flux and $\omega_e=\frac{eB_0}{m_ec}$.

§3. Dispersion Relations

3.1 Dispersion relation in electrostatic limit

We, first, consider the dispersion relation for the electrostatic limit case. In this case the dispersion relation of the rippling mode can be obtained by taking the limit $\omega ck_z/\omega_A^2<<1$ where the right hand side of eq. (2.6) becomes zoro. As a results the dispersion relation of the electrostatic rippling mode can be obtained from the coupled equations (2.4) and (2.10) as follows,

$$iv_{te}^2k_z[\tilde{\Phi}_1-1.71\tilde{T}_1]+\frac{3}{4}\nu_{e0}v_{e0z}\tilde{T}_1=0, \quad (3.1)$$
$$\left(\omega-\omega_{0z}+i\omega_\chi\right)\tilde{T}_1-\omega_T^*\tilde{\Phi}_1=0. \quad (3.2)$$

Then, the dispersion relation of electrostatic drift rippling mode is given by

$$\omega=(\omega_{0z}+1.71\omega_T^*)+i\left(\frac{3}{4}\frac{\nu_{e0}\omega_{0z}}{v_{te}^2k_z^2}\omega_T^*-\omega_\chi\right). \quad (3.3)$$

Ignoring the real part in this equation, the first term of the imaginary part corresponds to the growth rate of the purely electrostatic rippling mode[1,4] and the second term is the stabilization due to the parallel thermal conduction.

This shows that the rippling mode seems to couple linearly with the drift waves ($\omega\sim\omega_T^*$) in electrostatic limit where the ion polarization drift is ignored and parallel electron perturbed current is not taken into account. That is because the density perturbations are not important in the purely growing electrostatic rippling instability. The electron density fluctuations can take place in the presence of density gradient but the ion dynamics has to be considered to fulfill the quasi neutrality requirement. In this situation both ions and electrons have the electric drift and they move together satisfying the charge neutrality exactly.

If we introduce the electromagnetic effect the electromagnetic rippling mode is not completely separate from Alfven waves. The density perturbations give rise to Alfven wave propagation and the coupling between the Alfven waves and the electrostatic drift rippling mode take place in the presence of density perturbations due to ion polarization drift and the electron parallel perturbed motion which guarantee $\nabla\cdot\mathbf{j}=0$

even in the absence of density gradient. Then the rippling mode does not follow the electrostatic dispersion relation but includes magnetic perturbation effects as well.

We observe that equation (2.6) implies $\tilde{A}_1 = \alpha\tilde{\Phi}_1$ where $\alpha \neq 0$. Just for the sake of comparison, we substitute the parameters at $T = 40$ eV in this equation. Then we notice $\tilde{A}_1 \approx 0.3\tilde{\Phi}_1$ and therefore the magnetic energy density is not ignorable.

3.2 *Electromagnetic dispersion relation*

The dispersion relation of low frequency electromagnetic waves in a current carrying collisional plasma can be obtained by solving coupled equations (2.4), (2,6), (2.9) and (2.10). Since we are interested mainly in rippling type instabilities we, here, assume a flat density profile and we do not consider the density gradient driven drift dissipative modes for simplicity. Then, the set of coupled equations (2.4), (2,6), (2.9) and (2.10) yields the cubic order linear dispersion relation as follows:

$$B_{3r}\omega^3 + (B_{2r} + iB_{2i})\omega^2 + (B_{1r} + iB_{1i})\omega + (B_{0r} + iB_{0i}) = 0, \quad (3.4)$$

where

$$B_{0r} = b\omega_{te}^2\omega_{0z} + \omega_A^2\omega_{0z} + 1.71\omega_T^*\omega_A^2, \quad (3.5a)$$

$$B_{0i} = -b\omega_{te}^2\omega_\chi - \omega_A^2\omega_\chi + \frac{3}{4}\nu_{e0}\omega_{0z}\omega_T^*\omega_A^2\omega_{te}^{-2}, \quad (3.5b)$$

$$B_{1r} = \omega_T^*\omega_{0z} - (a-1)\frac{\nu_{e0}}{2}\omega_\chi - \omega_{te}^2 b + b\omega_{0z}^2 - \omega_A^2 - 1.14\rho_s^2k_y^2\omega_A^2, \quad (3.5c)$$

$$B_{1i} = -\omega_T^*\omega_\chi - (a-1)\frac{\nu_{e0}}{2}\omega_{0z} - b\omega_\chi\omega_{0z} - 0.5\rho_s^2k_y^2\nu_{e0}\omega_{0z}\omega_A^2\omega_{te}^{-2}, \quad (3.5d)$$

$$B_{2r} = -\omega_T^* - a\omega_{0z} - b\omega_{0z}, \quad (3.5e)$$

$$B_{2i} = a\omega_\chi + (a-1)\frac{\nu_{e0}}{2}, \quad (3.5f)$$

$$B_{3r} = a, \quad (3.5g)$$

and

$$a = 1 + \lambda_e^2k^2, \quad (3.5h)$$

$$b = \lambda_e^2k_y^2, \quad (3.5i)$$

$$k^2 = k_y^2 + k_z^2 \quad (3.5j)$$

$$\lambda_e = c/\omega_{pe}, \quad (3.5k)$$

$$\omega_{te} = v_{te}k_z. \quad (3.5l)$$

We solve this dispersion relation (3.4) numerically assuming laboratory plasma parameters $B_0 = 3T$, and $n = 10^{13}cm^{-3}$. Figure 1 shows the temperature dependence of the solutions of the dispersion relation (3.4); (a) the real frequency and (b) the growth rate. The other parameters are $k_y = 5\text{cm}^{-1}$, $k_z = 0.5 \times 10^{-3}\text{cm}^{-1}$, $v_{e0z} = 0.1v_{eth}$, and $\kappa_T = 0.1\text{cm}^{-1}$, respectively. We can see that only one of the three modes (solution 1) is highly unstable with a growth rate of the order of ω_{0z} at low temperatures ($T_e \leq 50eV$). This corresponds to the electromagnetic rippling mode with a relatively lower frequency and with significantly shorter e-folding time. We can see stabilization of this mode due to the parallel thermal conduction in higher temperature region ($T_e > 50eV$).

We compare the electromagnetic rippling mode (solution 1) with the electrostatic rippling mode obtained by eq. (3.3) in order to study the electromagnetic effects on the real frequency and growth rate of rippling mode. Figure 2 shows the comparisons of the real frequency and the growth rate between the electromagnetic and electrostatic rippling mode for two typical parameters. The comparisons of the real frequency and growth rate with $k_y = 5\text{cm}^{-1}$, $k_z = 0.5 \times 10^{-3}\text{cm}^{-1}$, $v_{e0z} = 0.1v_{eth}$, and $\kappa_T = 0.1\text{cm}^{-1}$, are shown in Fig 2-(a) and (b). We can see that the real frequency is slightly decreased due to the electromagnetic effect. Also the small difference in growth rate at the low temperature region can be seen. Fiuger 2-(c) and (d) show the comparisons in the case of $k_y = 15\text{cm}^{-1}$, $k_z = 1.0 \times 10^{-3}\text{cm}^{-1}$, $v_{e0z} = 0.2v_{eth}$, and $\kappa_T = 0.1\text{cm}^{-1}$, where the Alfven frequency is closer to the real frequency of the rippling mode. In this case the coupling between the rippleing mode and the Alfven wave becomes stronger and the difference with the electrostatic rippling mode is increased. Especially the electromagnetic effect destabilize in the higher temperature region ($T_e \sim 60$eV).

As a result we found that the purely electrostatic growing rippling modes turn out to be an oscillatory instability in a current carrying dissipative plasma. It is important to note that a purely growing electrostatic resistive mode can become an oscillatory instability due to the presence of pressure perturbations. The recent experiments on tokamak discharges[12,13] have observed significant level of magnetic fluctuations in the edge region. Therefore we expect that the purely growing electrostatic rippling mode can turn out to be an oscillatory electromagnetic instability for relatively shorter wavelengths.

We can also see the other two modes (Solution 2 and 3) in Fig. 1. These modes are the shear Alfven waves and highly damped at low temperatures due to the strong dissipation by particle collisions. We can recover this dissipative Alfven modes in the limit $\omega_T^* \to 0$ and $\omega_{0z} \to 0$ in eq. (3.1) as,

$$(1 + \lambda_e^2k^2)\omega^2 + i\frac{\nu_{e0}\lambda_e^2k_y^2}{2}\omega - \omega_A^2(1 + 1.14\rho_s^2k_y^2) = 0. \quad (3.6)$$

If we assume $\nu_{e0}\lambda_e^2k_y^2\omega^2 << \omega_A$ and ignore the dissipation term in this dispersion relation, we obtain the well-known dispersion relation for the kinetic Alfven waves as well as the slow shear Alfven waves,

$$\omega^2 = \frac{\omega_A^2(1 + \rho_s^2k_y^2)}{1 + \lambda_e^2k^2}. \quad (3.7)$$

As a result we find that the shear Alfven waves are highly damped in the low temperature edge region, even in the presence of temperature gradient and external current.

§4. Parameter Dependency of Electromagnetic Rippling Mode

In the previous section we have studied three coupled modes in the dispersion relation (3.4). One is the electromagnetic rippling mode and the other two are the shear Alfven waves which are highly damped. Here, the parameter dependency of the electromagnetic rippling mode is investigated changing the wave and plasma parameters.

We, first, study the wave number dependency on the growth rate of the electromagnetic rippling mode. Figure 3 shows the comparison of the real frequency (a) and the growth rate (b) of

the rippling mode with following four sets of parallel and perpendicular wave number values, k_z and k_y; (A) $k_y = 5\text{cm}^{-1}$ and $k_z = 0.5 \times 10^{-3}\text{cm}^{-1}$, (B) $k_y = 5\text{cm}^{-1}$ and $k_z = 1.0 \times 10^{-3}\text{cm}^{-1}$, (C) $k_y = 10\text{cm}^{-1}$ and $k_z = 0.5 \times 10^{-3}\text{cm}^{-1}$, and (D) $k_y = 10\text{cm}^{-1}$ and $k_z = 1.0 \times 10^{-3}\text{cm}^{-1}$. The electron temperature gradient and parallel flow velocity are chosen such that $\kappa_T = 0.1\text{cm}^{-1}$ and $v_{e0z} = 0.1 v_{eth}$, respectively.

We can see that the real frequency depend on both of k_z and k_y. The k_y dependency of the real frequency can be understand by the strong dependency on the drift wave frequency, ω_T^*, and the k_z dependency comes from the change of normalization factor $\omega_{z0}(= v_{e0z}k_z)$. The growth rate also shows the dependency on both of k_z and k_y. The mode is most unstable in the case of smaller k_z and larger k_y values.

Next, we study the density and the magnetic field strength dependency on the electromagnetic rippling mode. Figure 4 shows the real frequency and the growth rate as a function of electron temperature with changing the density and magnetic field strength. We can see the weak dependency of the real frequency on the density but the strong dependency of the growth rate on the density [Fig. 4 (a) and (b)]. The strong dependency of the real frequency on the magnetic field strength can be seen in Fig 4-(c), especially in the higher temperature region. Also it is found that the mode is more unstable in the weak magnetic field, where the ω_T^* increases.

The electron temperature gradient, κ_T, and the electron parallel flow, v_{e0z}, are also important parameters for the growth of rippling instability. We, next, study the dependencies of the electron temperature gradient and the electron parallel flow on the growth rate of rippling mode. Figure 5 shows the real frequency and the growth rate of the rippling mode as a function of the electron temperature gradient for two different parameters assumed in Fig. 2 (weak and strong coupling cases); (A) $k_y = 5\text{cm}^{-1}$, $k_z = 0.5 \times 10^{-3}\text{cm}^{-1}$ and $v_{e0z} = 0.1 v_{eth}$, and (B) $k_y = 15\text{cm}^{-1}$, $k_z = 1.0 \times 10^{-3}\text{cm}^{-1}$ and $v_{e0z} = 0.2 v_{eth}$. The electron temperature is assumed to be $T_e = 30\text{eV}$.

The increase of growth rate can be seen as κ_T increases and the mode becomes unstable when $\kappa_T \sim 0.03\text{cm}^{-1}$. The increase of κ_T enlarges ω_T^* and the growth rate rises in the higher κ_T. Interestingly the saturation of the real frequency and the growth rate can be seen in the strong coupling case.

Figure 6 shows the electron parallel flow dependency on the growth rate of the rippling mode. The electron temperature and the electron temperature gradient are assumed to be $T_e = 80\text{eV}$ and $k_T = 0.1\text{cm}^{-1}$, respectively. The other parameters of (A) and (B) are same as in Fig. 5. We can see the strong increase of the growth rate as v_{e0z} increases in the lower v_{e0z} region ($v_{e0z}/v_{eth} < 0.1$) while this increment of the growth rage suppressed in the higher v_{e0z} region. We can not see any difference of the tendency between the weak coupling and strong coupling cases.

§5. Summary

We have shown that electromagnetic perturbations can be associated with the rippling mode instability to explain one of the causes of low frequency electromagnetic fluctuations observed in tokamak edge regions particularly in shorter wavelength regime. The purely electrostatic growing rippling mode can appear as an oscillatory electromagnetic instability. It is noticed that this instability can not occur in hot regions of the plasma. As the temperature increases this electromagnetic perturbation damps very rapidly. Since the mode has non vanishing parallel wave vector therefore parallel thermal conduction equalizes the temperature as it increases. This phenomenon is similar to the electrostatic rippling instability.

Our analysis shows that the electrostatic drift rippling mode can couple with Alfven waves in current carrying resistive plasmas. The electrostatic drift rippling mode is considered to be a longer wavelength perturbation such that $\lambda^2 k^2 << 1$ and $\kappa_T \sim 0.1$. In case of shorter wavelength perturbations for which $\lambda k \sim 1$ and $\kappa_T \sim 0.1$, we think the electromagnetic effects should not be ignored completely. In this case the rippling mode is coupled with electromagnetic Alfven waves as well. The real frequency of the electromagnetic rippling mode remains below the Alfven frequency. But as we have shown that the level of the fluctuation of magnetic vector potential can be about one third of electrostatic potential. In this case the electromagnetic effects should be taken into account and this study can explain a possible cause of relatively shorter wavelength fluctuations observed in the tokamak edges.

In the plasma edge regions with relatively low temperatures ($T_e \leq 50eV$), the temperature gradient would become steep and electromagnetic rippling instability can take place giving rise to particle and energy transport. This mode can couple with the electromagnetic and electrostatic drift dissipative waves in the presence of density gradient. However the large magnetic shear in tokamak edge region enlarges the parallel wave vector, k_z, and would stabilize this mode.

In this study we have discussed the electromagnetic effects on the rippling mode with local approximation. The non-local effect (e.g. magnetic shear) would also have some influence on the rippling mode. Hassam and Drake[4] considered the non-local effects on the rippling mode but in the electrostatic limit. Electromagnetic case is more complicated due to the effects of parallel vector potential and this is our future work. Also we have assume the flat density profile in this analysis. The density gradient also have significant effects on the rippling mode. This would be discussed in the different paper.

Acknowledgments

One of us (H.S.) would like to thank the Japan Society for the Promotion of Science (JSPS) for the award of the fellowship, and Professor T. Sato for the hospitality at the National Institute for Fusion Science, Japan. The authors are grateful to Professor K. Watanabe for several useful discussions and to Professor M. Okamoto for continuous encouragement.

1) H. P. Furth, J Killeen and M.N Rosenbluth: Phys Fluids **6** (1963) 459
2) L. Garcia, J D. Callen, B. A.Carreras, P. H Diamond, and H R. Hicks: Bull. Am. Phys Soc. **26** (1981) 1061.
3) B Coppi: Phys. Fluids **8** (1965) 2273.
4) A. B. Hassam, and J. F. Drake· Phys. Fluids **26** (1983) 133.
5) Ch. P Ritz, R.V. Brarvenec, P.M. Schoch, R.D Bengton, J A.Boedo, J.C. Forcter, K W. Gentle, Y. He, R.L. Hickok, Y.J. Kim, H. Lin, P. E. Philips, T.L. Rhodes, W. L.Rowan, P. M. Valauju, and A. J Wootton: Phys. Rev. Lett **62** (1989) 1844.
6) Y. J. Kim, K. W. Gentle, C. E. Ritz, T. L. Rhodes, and R. D. Bengston: Nucl. Fusion **29** (1989) 99.
7) N. Ohyabu, J. H. Osborne, G. L. Jahns, E J. Strait, and R. D Stambaugh: Nucl. Fusion **29** (1989) 475.
8) C. Hidalgo, M. A. Pedrosa, A. P. Navarro, F.L. Tabares, E. Ascasibar and F. Perez Murano: Nucl. Fusion **30** (1990) 717.
9) H. Y. W. Tsui, H. Lin, M. Meir, and A. J. Wootton: in Proceedings of the Eighteenth Conference on Controlled Fusion and Plasma Physics,

Berlin, edited by P Bachmann and D C Robinson (European Physical Society , Petit-Lancy, Switzerland **15c** (1991) 297
10) S I Braginskii *Reviews of Plasma Physics*, edited by M A Leontovich (Consultants Bureau, New York, 1965),Vol I,p 205
11) H Saleem, and P K Shukla, Phys Plasmas **B4** (1992) 86
12) G Vayakis, Nuclear Fusion **33** (1993) 547
13) R Nazikian, Z Chang, E D Fredrickson, E Mazzucato, S H Batha, R Bell, R Budny, C E. Bush, C Z Cheng, A Janos, F. Levinton, J Manickam, D K Mansfield, H K Park, G Rewoldt, S. Sabbagh, E J Synakowski, W Tang, G Taylor, and L E Zakharov, Phys Plasmas **3** (1996) 593

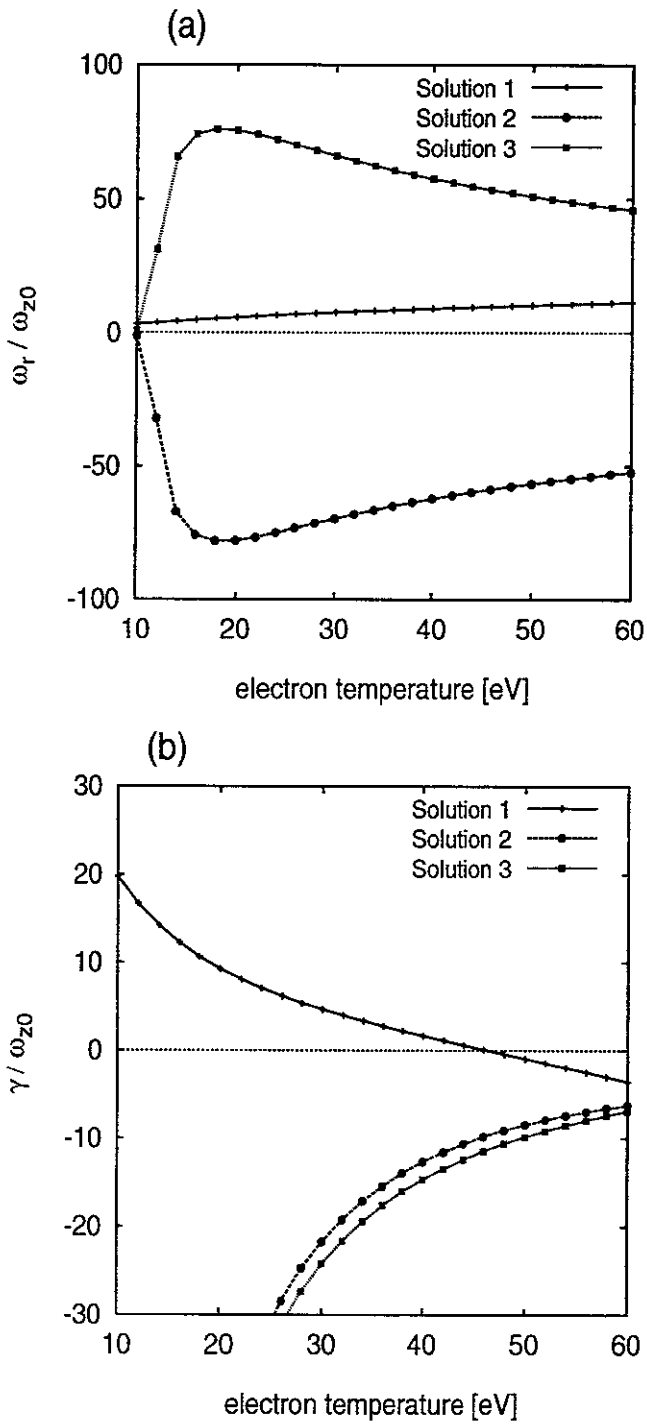

Fig. 1 : Three solutions of the dispersion relation eq. (3.4) as a function of electron temperature; (a) real frequency and (b) growth rate.

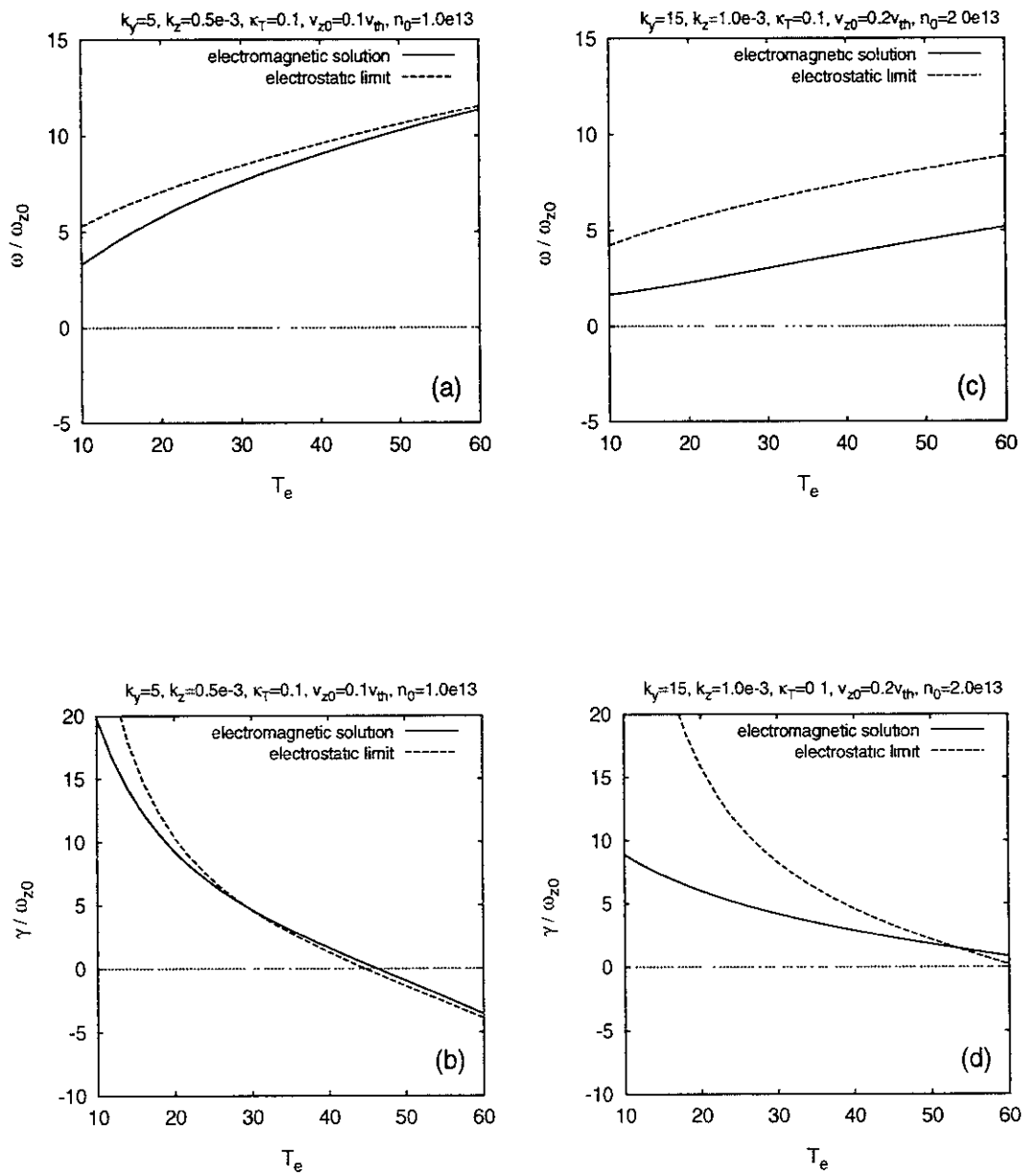

Fig. 2 : Comparisons of the real frequency and the growth rates for the electrostatic and electromagnetic rippling modes with two different parameter cases (weak and strong coupling with Alfven wave).

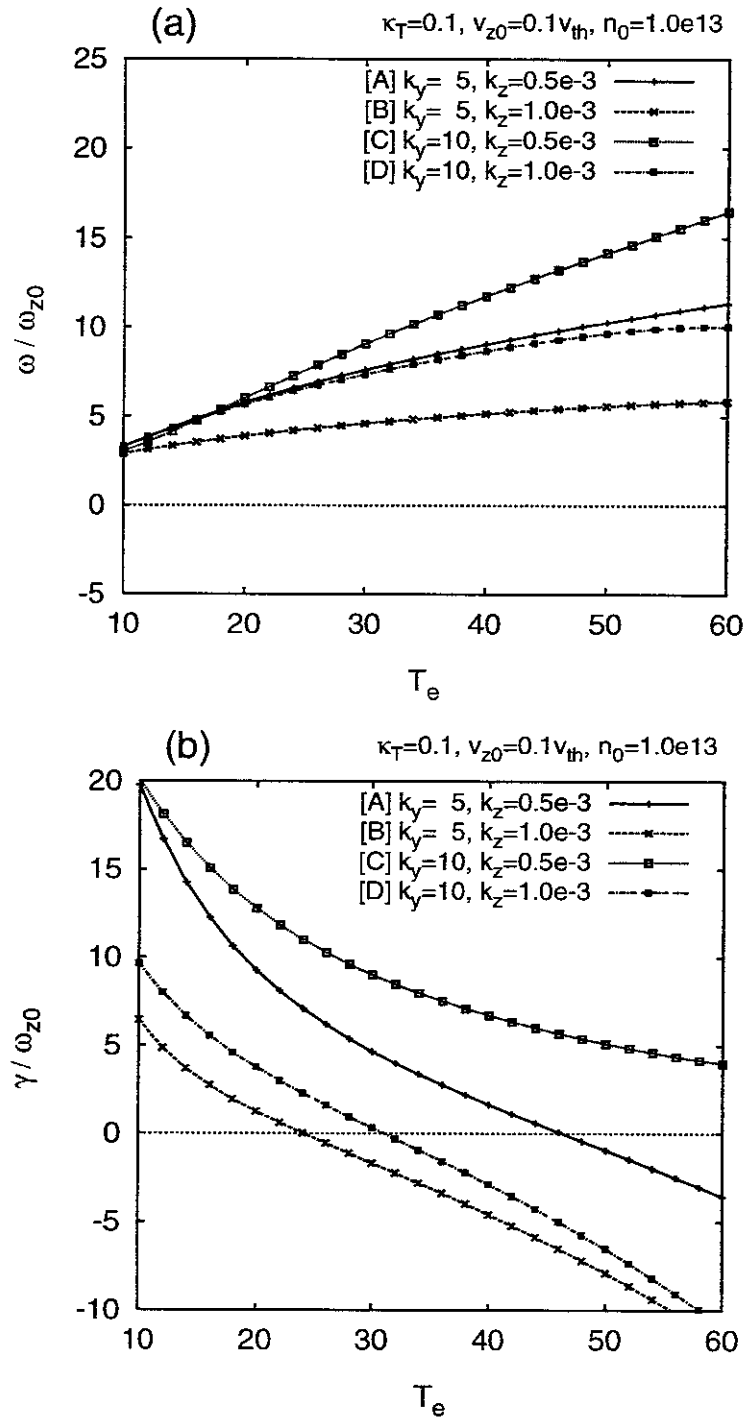

Fig. 3 : Plots of the real frequency and the growth rates of the electromagnetic rippling mode changing the parallel and perpendicular wave number values, k_z and k_y, as a function of electron temperature.

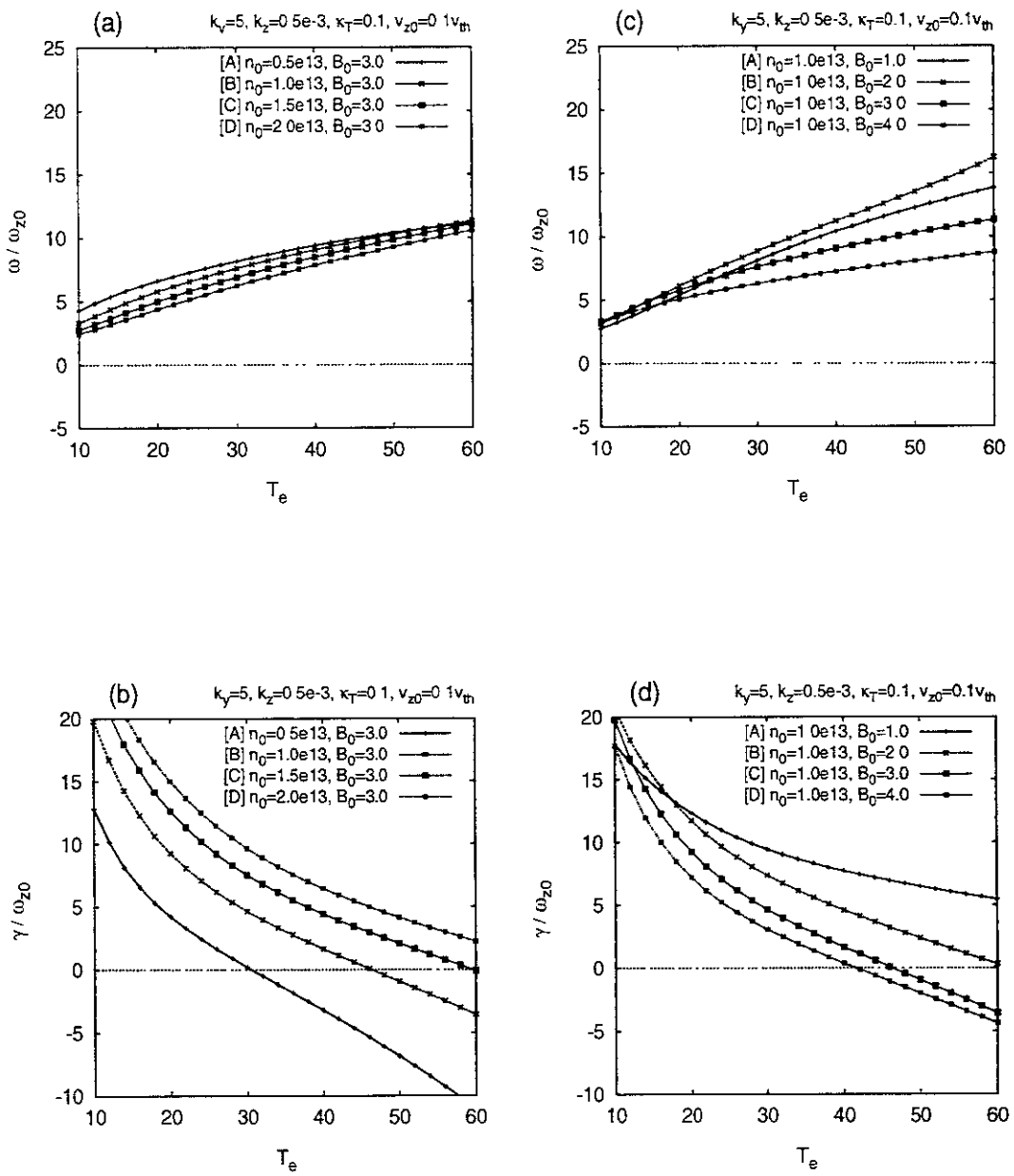

Fig. 4 : Plots of the real frequency and the growth rate for the different density, (a) and (b), and the magnetic field strength, (c) and (d), as a function of the electron temperature.

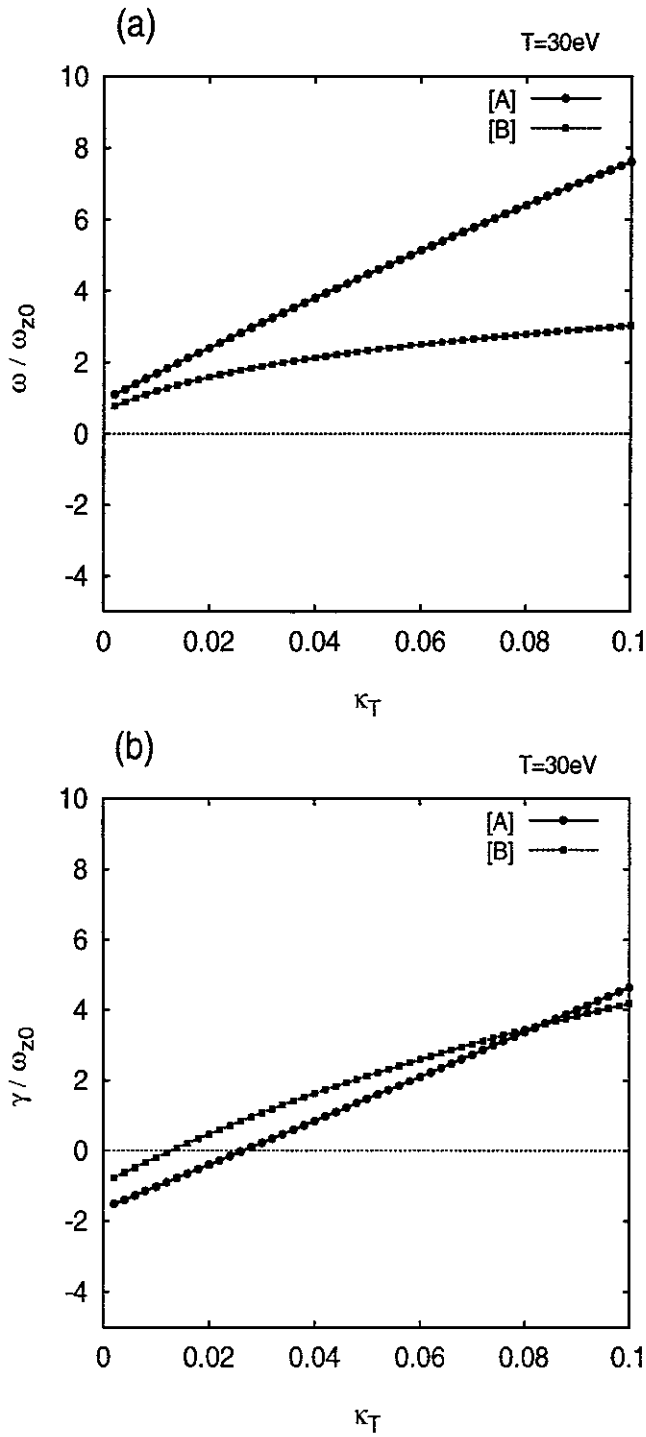

Fig. 5 : Plots of the real frequency and the growth rate as a function of th electron temperature gradient, k_T, with two different parameter cases (the weak and strong coupling with Alfven wave cases in Fig 2).

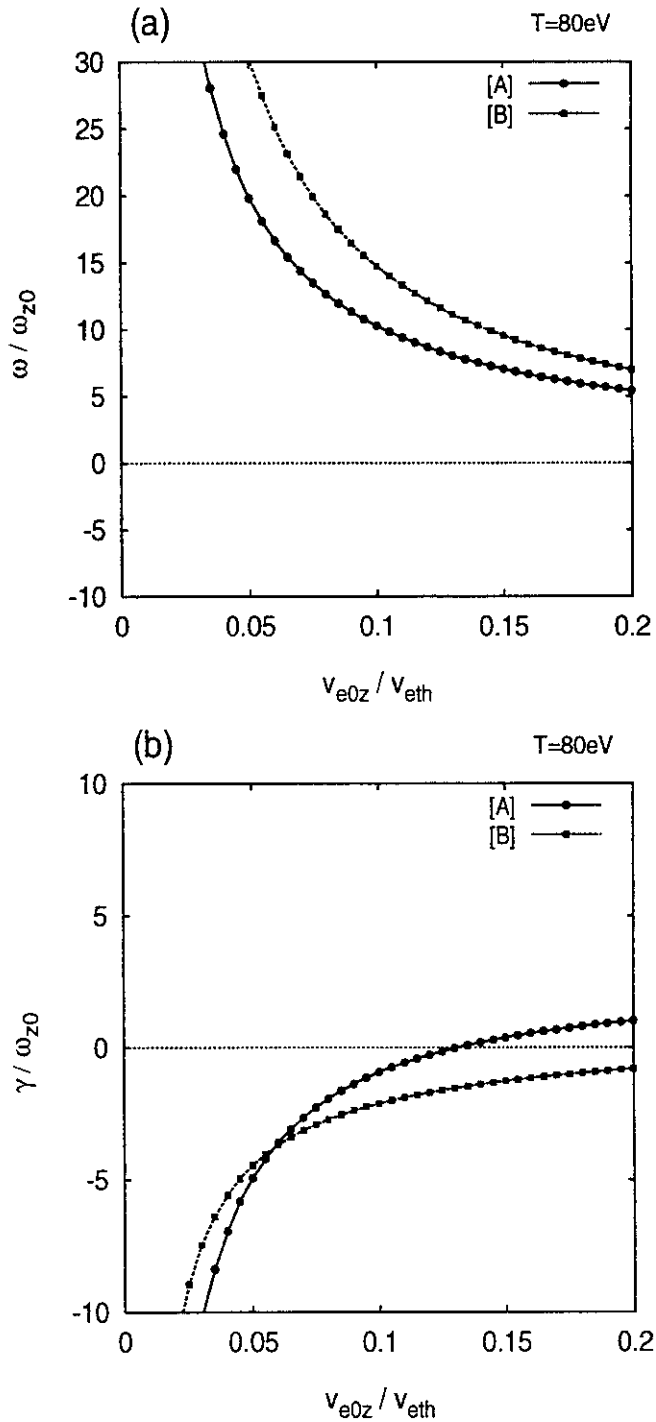

Fig. 6 : Plots of the real frequency and the growth rate as a function of electron parallel flow with two different parameter cases (the weak and strong coupling with Alfven wave cases in Fig 2).

Recent Issues of NIFS Series

NIFS-518 J. Chen, N. Nakajima and M. Okamoto,
Shift-and-Inverse Lanczos Algorithm for Ideal MHD Stability Analysis, Nov. 1997

NIFS-519 M. Yokoyama, N. Nakajima and M. Okamoto,
Nonlinear Incompressible Poloidal Viscosity in L=2 Heliotron and Quasi-Symmetric Stellarators, Nov 1997

NIFS-520 S. Kida and H. Miura,
Identificaiton and Analysis of Vortical Structures, Nov. 1997

NIFS-521 K. Ida, S. Nishimura, T. Minami, K. Tanaka, S. Okamura, M. Osakabe, H. Idei, S. Kubo, C. Takahashi and K. Matsuoka,
High Ion Temperature Mode in CHS Heliotron/torsatron Plasmas; Nov. 1997

NIFS-522 M. Yokoyama, N. Nakajima and M. Okamoto,
Realization and Classification of Symmetric Stellarator Configurations through Plasma Boundary Modulations, Dec. 1997

NIFS-523 H. Kitauchi,
Topological Structure of Magnetic Flux Lines Generated by Thermal Convection in a Rotating Spherical Shell; Dec. 1997

NIFS-524 T. Ohkawa,
Tunneling Electron Trap, Dec. 1997

NIFS-525 K. Itoh, S.-I. Itoh, M. Yagi, A. Fukuyama,
Solitary Radial Electric Field Structure in Tokamak Plasmas, Dec. 1997

NIFS-526 Andrey N. Lyakhov,
Alfven Instabilities in FRC Plasma; Dec. 1997

NIFS-527 J. Uramoto,
Net Current Increment of negative Muonlike Particle Produced by the Electron and Positive Ion Bunch-method; Dec. 1997

NIFS-528 Andrey N. Lyakhov,
Comments on Electrostastic Drift Instabilities in Field Reversed Configuraiton; Dec. 1997

NIFS-529 J. Uramoto,
Pair Creation of Negative and Positive Pionlike (Muonlike) Particle by Interaction between an Electron Bunch and a Positive Ion Bunch; Dec. 1997

NIFS-530 J. Uramoto,
Measuring Method of Decay Time of Negative Muonlike Particle by Beam Collector Applied RF Bias Voltage, Dec. 1997

NIFS-531 J. Uramoto,
Confirmation Method for Metal Plate Penetration of Low Energy Negative Pionlike or Muonlike Particle Beam under Positive Ions, Dec. 1997

NIFS-532 J. Uramoto,
Pair Creations of Negative and Positive Pionlike (Muonlike) Particle or K Mesonlike (Muonlike) Particle in H2 or D2 Gas Discharge in Magnetic Field, Dec. 1997

NIFS-533 S. Kawata, C. Boonmee, T. Teramoto, L. Drska, J. Limpouch, R. Liska, M. Sinor,
Computer-Assisted Particle-in-Cell Code Development; Dec. 1997

NIFS-534 Y. Matsukawa, T. Suda, S. Ohnuki and C. Namba,
Microstructure and Mechanical Property of Neutron Irradiated TiNi Shape Memory Alloy; Jan. 1998

NIFS-535 A. Fujisawa, H. Iguchi, H. Idei, S. Kubo, K. Matsuoka, S. Okamura, K. Tanaka, T. Minami, S. Ohdachi, S. Morita, H. Zushi, S. Lee, M. Osakabe, R. Akiyama, Y. Yoshimura, K. Toi, H. Sanuki, K. Itoh, A. Shimizu, S. Takagi, A. Ejiri, C. Takahashi, M. Kojima, S. Hidekuma, K. Ida, S. Nishimura, N. Inoue, R. Sakamoto, S.-I. Itoh, Y. Hamada, M. Fujiwara,
Discovery of Electric Pulsation in a Toroidal Helical Plasma; Jan. 1998

NIFS-536 Lj.R. Hadzievski, M.M. Skoric, M. Kono and T. Sato,
Simulation of Weak and Strong Langmuir Collapse Regimes; Jan. 1998

NIFS-537 H. Sugama, W. Horton,
Nonlinear Electromagnetic Gyrokinetic Equation for Plasmas with Large Mean Flows; Feb. 1998

NIFS-538 H. Iguchi, T.P. Crowley, A. Fujisawa, S. Lee, K. Tanaka, T. Minami, S. Nishimura, K. Ida, R. Akiyama, Y. Hamada, H., Idei. M. Isobe, M. Kojima, S. Kubo, S. Morita, S. Ohdachi, S. Okamura, M. Osakabe, K. Matsuoka, C. Takahashi and K. Toi,
Space Potential Fluctuations during MHD Activities in the Compact Helical System (CHS); Feb. 1998

NIFS-539 Takashi Yabe and Yan Zhang,
Effect of Ambient Gas on Three-Dimensional Breakup in Coronet Formation Process; Feb. 1998

NIFS-540 H. Nakamura, K. Ikeda and S. Yamaguchi,
Transport Coefficients of InSb in a Strong Magnetic Field; Feb. 1998

NIFS-541 J. Uramoto,
Development of ν_μ Beam Detector and Large Area ν_μ Beam Source by H_2 Gas Discharge (I); Mar. 1998

NIFS-542 J. Uramoto,
Development of $bar\{\nu\}_\mu$ Beam Detector and Large Area $bar\{\nu\}_\mu$ Beam Source by H_2 Gas Discharge (II); Mar. 1998

NIFS-543 J. Uramoto,
Some Problems inside a Mass Analyzer for Pions Extracted from a H_2 Gas Discharge; Mar. 1998

NIFS-544 J. Uramoto,
Simplified ν_μ $bar\{\nu\}_\mu$ Beam Detector and ν_μ $bar\{\nu\}_\mu$ Beam Source by Interaction between an Electron Bunch and a Positive Ion Bunch; Mar. 1998

NIFS-545 J. Uramoto,
Various Neutrino Beams Generated by D_2 Gas Discharge; Mar.1998

NIFS-546 R. Kanno, N. Nakajima, T. Hayashi and M. Okamoto,
Computational Study of Three Dimensional Equilibria with the Bootstrap Current; Mar. 1998

NIFS-547 R. Kanno, N. Nakajima and M. Okamoto,
Electron Heat Transport in a Self-Similar Structure of Magnetic Islands; Apr 1998

NIFS-548 J.E. Rice,
Simulated Impurity Transport in LHD from MIST; May 1998

NIFS-549 M.M. Skoric, T. Sato, A.M. Maluckov and M.S. Jovanovic,
On Kinetic Complexity in a Three-Wave Interaction; June 1998

NIFS-550 S. Goto and S. Kida,
Passive Saclar Spectrum in Isotropic Turbulence: Prediction by the Lagrangian Direct-interaction Approximation; June 1998

NIFS-551 T. Kuroda, H. Sugama, R. Kanno, M. Okamoto and W. Horton,
Initial Value Problem of the Toroidal Ion Temperature Gradient Mode ; June 1998

NIFS-552 T. Mutoh, R. Kumazawa, T. Seki, F. Simpo, G. Nomura, T. Ido and T. Watari,
Steady State Tests of High Voltage Ceramic Feedthoughs and Co-Axial Transmission Line of ICRF Heating System for the Large Helical Device ; June 1998

NIFS-553 N. Noda, K. Tsuzuki, A. Sagara, N. Inoue, T. Muroga,
oronaization in Future Devices -Protecting Layer against Tritium and Energetic Neutrals-: July 1998

NIFS-554 S. Murakami and H. Saleem,
Electromagnetic Effects on Rippling Instability and Tokamak Edge Fluctuations; July 1998